ACES Asian Chemical Editorial Society
DOI: 10.1002/asia.201700151
CHEMISTRY AN ASIAN JOURNAL
Full Paper

Oligogermanes

SPECIAL ISSUE

Molecular Oligogermanes and Related Compounds: Structure, Optical and Semiconductor Properties

Kirill V. Zaitsev,*[a] Viktor A. Tafeenko,[a] Yuri F. Oprunenko,[a] Anastasia V. Kharcheva,[a] Zhaisan Zhanabil,[b] Yerlan Suleimen,[b] Kevin Lam,*[b] Vladimir B. Zaitsev,[c] Anna V. Zaitseva,[d] Galina S. Zaitseva,[a] and Sergey S. Karlov[a]

Abstract: The optical (UV/Vis absorbance, fluorescence in the solid state and in solution) and semiconducting properties of a number of di- and trigermanes as well as related silicon- and tin-containing germanes, **1**–**6** ((*p*-Tol)$_3$GeGeMe$_3$ (**1**), Ph$_3$SnGe(SiMe$_3$)$_3$ (**2**), (C$_6$F$_5$)$_3$GeGePh$_3$ (**3**), (*p*-Tol)$_3$GeSiMe$_2$SiMe$_3$ (**4**), (*p*-Tol)$_3$GeGeMe$_2$Ge(*p*-Tol)$_3$ (**5**), (*p*-Tol)$_3$GeSiMe$_2$SiMe$_2$Ge(*p*-Tol)$_3$ (**6**)) were investigated. Molecular structures of **5** and **6** were studied by X-ray diffraction analysis. All compounds displayed luminescence properties. In addition, a band gap (of about 3.3 eV) was measured for compounds **1**–**6** showing that those molecules display semiconductor properties.

Introduction

Catenated oligosilanes[1] and oligogermanes[2] are attracting the attention of the scientific community due to their unique physical properties. These compounds possess strong UV/Vis absorption, luminescence, and photo- and electric conductivity due to the presence of an effective σ-conjugation between the group 14 elements (E = Si, Ge, Sn, Pb). Special attention should be paid to germanium compounds since they exhibit semiconducting properties due to their smaller band gap and higher electron and hole mobilities.

[a] Dr. K. V. Zaitsev, Dr. V. A. Tafeenko, Dr. Y. F. Oprunenko, A. V. Kharcheva, Dr. G. S. Zaitseva, Prof. S. S. Karlov
Department of Chemistry
Moscow State University
Leninskye Gory, 1, 3, Moscow 119991 (Russia)
E-mail: zaitsev@org.chem.msu.ru

[b] Z. Zhanabil, Dr. Y. Suleimen, Dr. K. Lam
Department of Chemistry
School of Science and Technology
Nazarbayev University
Astana, 010000 (Kazakhstan)
E-mail: kevin.lam@nu.edu.kz

[c] Dr. V. B. Zaitsev
Department of Physics
Moscow State University
Leninskye Gory, 1, Moscow 119991 (Russia)

[d] Dr. A. V. Zaitseva
Institute of Physical Chemistry
Russian Academy of Sciences
Leninskii pr. 31, Moscow (Russia)

Supporting information and the ORCID identification number(s) for the author(s) of this article can be found under http://dx.doi.org/10.1002/asia.201700151.

This manuscript is part of a special issue on advances in silicon chemistry. Click here to see the Table of Contents of the special issue.

Semiconducting properties in polymeric catenated group 14 derivatives are usually observed after the molecules have undergone a special treatment such as an oxidative doping by SbF$_5$ or AsF$_5$.[3] In this case, partial oxidation results in the formation of a cation radical, similar to the "hole" usually found in elemental Si or Ge, and leads to a positive charge mobility within the elemental chain itself. In fact, polygermanes/polysilanes intrinsically display photoconductivity in which the electron transport is assured by a hole-hopping process. Such as phenomenon strongly depends on the nature and on the length of the side-chain.[4] The construction of semiconducting devices based on such polymer materials[5] (polysilanes, polygermanes, polystannanes) relies on specific techniques, such as the production of doped thin films.[6] Interestingly, the band gap in elemental Ge is lower than the one in Si, and hence one could expect enhanced conductive properties in individual germanium organic compounds. Therefore, the synthesis and the studies of the shortest group 14 element chain (especially containing Ge atoms) which is necessary for the conductive properties to be observed may be regarded as an essential task in the development of new semiconducting devices based on germanium. The conductivity mechanism in free oligogermanes and related compounds is significantly different from the one observed in other related conductive materials due to σ-bond electron delocalization.[7] In oligogermanes, it is well known that the HOMO is distributed across the chain of group 14 elements,[2] and an interchain hopping mechanism has been previously described.[5]

Investigations and studies of small molecules and their properties should help to establish a structure–property relationship. Recently, several works emerged in which single-molecule conductance has been studied.[8] However, in such studies a very specific and complex method (scanning tunneling mi-

© 2017 Wiley-VCH Verlag GmbH & Co. KGaA, Weinheim

croscope-based break-junction) was used to measure the conductance.

In continuation of our research program on catenated germanium compounds[9] we perform this detailed investigation. Taking into account that oligogermanes as well as related silicon- and tin-containing germanes include semiconducting (silicon and germanium) atoms, we decided to investigate the optical and semiconductor properties of several molecular organometallic compounds (**1**–**6**) in their solid state. The optical and electrochemical properties of oligogermanes were also investigated in solution. Thus, this research contains subjects from various fields of science including not only various branches of chemistry (synthesis, studying the structure, electrochemistry) but also spectroscopy (NMR, UV/vis), physics, and materials science.

Results and Discussion

Several types of compounds were investigated in this work. Germanes (*p*-Tol)$_3$Ge-GeMe$_3$ (**1**), Ph$_3$Sn-Ge(SiMe$_3$)$_3$ (**2**)[9e] and (C$_6$F$_5$)$_3$Ge-GePh$_3$ (**3**)[9d] were prepared using known procedures. Compounds **4**–**6** were prepared by reacting (*p*-Tol)$_3$GeLi, formed in situ, with a silicon or germanium halide (Scheme 1). They were isolated in good yields as white crystalline air- and moisture-stable powders, soluble in common organic solvents (toluene, ether, chloroform, THF).

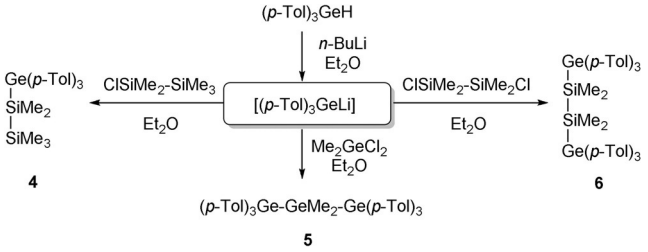

Scheme 1. Synthesis of compounds **4**–**6**.

The structures of compounds **5** and **6** in the solid state were studied by X-ray analysis (Figures 1 and 2; Table S1, Supporting Information); in solution, the structures of those novel derivatives were investigated by multinuclear NMR (see Supporting Information, Figures S1–S11), UV/Vis and emission spectroscopies as well as by electrochemistry. For comparison purposes, the luminescent properties of compounds **1**–**3** were also studied.

To the best of our knowledge, only 10 structures of linear trigermanes have been reported so far (Table 1). The steric hindrance and the electronic properties of the substituents (electron donors or acceptors) are the main factors that impact the structural parameters of oligogermanes.

The crystal structure of compound **5** is highly symmetric and displays a C_{2v} symmetry. The geometry at each Ge atom may be described as a slightly distorted tetrahedron. The substituents at the neighboring Ge atoms are in an *anti*-conformation (the average value of the torsion angle C-Ge(1)-Ge(2)-C is

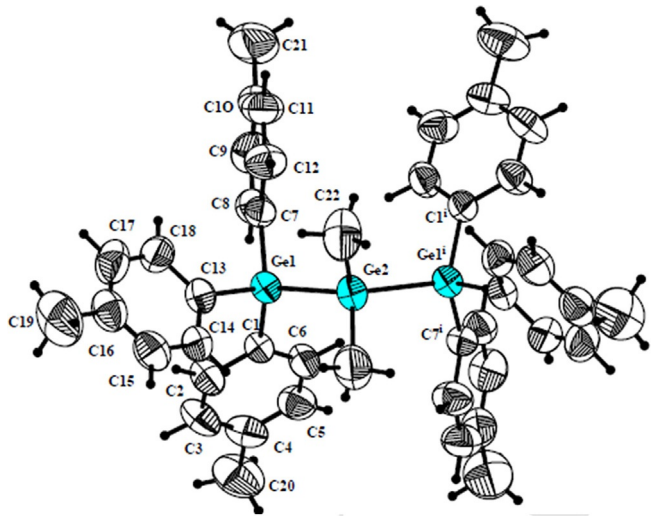

Figure 1. Molecular structure of **5**. Displacement ellipsoids are shown at 50% probability level. Selected bond lengths (Å) and bond angles (deg): Ge–Ge 2.4219(6), Ge(1)–C$_{av}$ 1.949(4), Ge(2)–C(22) 1.941(5); C-Ge(1)-C$_{av}$ 108.39(19), C-Ge(1)-Ge(2)$_{av}$ 110.46(12), C(22)-Ge(2)-C(22i) 106.5(4), C-Ge(2)-Ge(1)$_{av}$ 107.32(17), Ge(1)-Ge(2)-Ge(1i) 120.37(4).

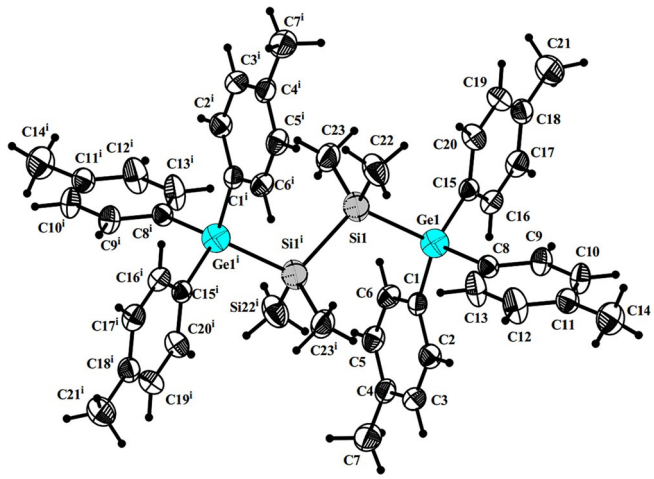

Figure 2. Molecular structure of **6**. Displacement ellipsoids are shown at 50% probability level. Selected bond lengths (Å) and bond angles (deg): Ge(1)–Si(1) 2.3972(10), Si(1)–Si(1i) 2.3486(18), Ge(1)–C$_{av}$ 1.952(3), Si(1)–C$_{av}$ 1.871(3); C-Ge(1)-C$_{av}$ 107.29(13), C-Ge(1)-Si(1)$_{av}$ 111.56(9), C(22)-Si(1)-C(23) 108.6(2), C-Si(1)-C$_{av}$109.77(14), C(22)-Si(1)-Ge(1) 108.51(14), Si(1i)-Si(1)-Ge(1) 110.31(5).

175.76(19)°). The value of Ge(1)-Ge(2)-Ge(1i) (120.37(4)°) angle is close to 120°,[10] which indicates an efficient delocalization of σ-electron density between the Ge atoms. In general the structural parameters of **5** are very close to those of (*p*-Tol)$_3$Ge-GeMe$_3$, **1**.[9e] At the same time, **5** displays the shortest Ge–Ge bond length among the known trigermanes investigated by X-ray analysis.

The molecular structure of compound **6** is centrosymmetric (space group $P\bar{1}$, $Z=1$). The structural parameters are very close to those found for (*p*-Tol)$_3$Ge-SiMe$_3$.[9e] In **6**, the substituents along the Ge–Si bond in (*p*-Tol)$_3$Ge-SiMe$_2$ fragment are in a skewed conformation[10b] (torsion angle C-Ge-Si-C is

© 2017 Wiley-VCH Verlag GmbH & Co. KGaA, Weinheim

Table 1. Main structural parameters of trigermanes investigated by X-ray analysis.

Trigermane	d(Ge-Ge)$_{av}$ [Å]	Angle Ge-Ge-Ge$_{av}$, deg	Angle C-Ge$_{central}$-C$_{av}$, deg	Reference
$[Ph_3Ge]_2GePh_2$	2.440(2)	121.3(1)	108.7(4)	[11]
$[Ph_3Ge]_2GeMe_2$	2.429(1)	120.3(1)	109.2(2)	[12]
$[ClPh_2Ge]_2GePh_2$	2.423(4)	113.52(12)	111.82(13)	[13]
$[Me(t\text{-}Bu)_2Ge]_2Ge(t\text{-}Bu)_2$	2.620(3)	118.56(17)	110.31(15)	[14]
$[Br(t\text{-}Bu)_2Ge]_2Ge(t\text{-}Bu)_2$	2.609(2)	113.61(15)	109.25(12)	[14]
$[I(t\text{-}Bu)_2Ge]_2Ge(t\text{-}Bu)_2$	2.641(1)	115.38(10)	109.36(12)	[15]
$[(p\text{-}Tol)_3Ge]_2GePh_2$	2.4328(5)	114.80(2)	106.2(1)	[16]
$[(p\text{-}Tol)_3Ge]_2Ge(p\text{-}Tol)_2$	2.4404(5)	117.54(1)	106.45(9)	[16]
$[(p\text{-}Tol)_3Ge]_2Ge(C_6F_5)_2$	2.459(5)	124.10(3)	108.0(2)	[9d]
$[(Me_3Si)_3Ge]_2GeMe_2$	2.4616(8)	125.00(4)	105.35(6)	[17]
$[(p\text{-}Tol)_3Ge]_2GeMe_2$ (**5**)	2.4219(6)	120.37(4)	106.5(4)	this work

86.58(14)°). At the same time the geometry along the Me_2Si-$SiMe_2$ fragment may be described as an ideal *anti*-conformation (torsion angle Ge-Si-Si-Ge is 180.00(5)°). Such a conformation allows for an effective σ-conjugation in the chain of four atoms of group 14 elements.

Only three compounds with a related structure have been reported so far (Table 2). When comparing the structural parameters of **6** with the related compounds shown in Table 2, it is evident that the steric volume of the substituents plays a key role in the geometry of such molecules. Introduction of bulky groups, even at the ends of the elemental chain, leads to a noticeable increase in bond lengths.

The chemical shifts in the NMR spectra of related *p*-tolyl-substituted Ge and Si derivatives **4**–**6** are very similar. There are two doublets in the aromatic region (at δ 7.32–7.18 and 7.15–7.03 ppm with 7.8 Hz spin-coupling constant) and a singlet of the methyl group (at approximately δ 2.35 ppm). Very similar signals of *C*H groups are observed in the ^{13}C NMR spectra (at approximately δ 135.4, 128.9 ppm), typical for *para*-substituted tolyl group, but the *ipso*-carbons (at δ 137.9 and 134.6–135.2 ppm) are more sensitive to the nature of substituent.

The topology of the single-crystal surface of compounds **1**, **2** and **5** was investigated by atomic force microscopy (AFM). Figures 3 and 4 show the AFM data for compound **1** (for other compounds, see the Supporting Information, Figures S12–S17). As it can be seen from Figure 3, the corresponding growth steps may be easily measured. Plotting of the surface cross-sections allows estimating the height of these growth steps. Figure 4 shows an analysis of the surface profile of compound **1** for one of the investigated sites.

The analysis of cross-sections obtained with several samples of the same compound provides an average value of 1.46 ± 0.01 nm for the step height growth. Such a value correlates with the size of the elemental cell (a:b:c = 10.6888(2):19.3569(4):12.2900(3) Å) of **1** according to the X-ray data.[9e] In the case of **2**, the step height growth is 0.97 ± 0.03 nm.

The UV/Vis absorbance spectra of compounds **4**–**6** in solution are given in Figure 5.

The data concerning the UV/Vis absorption of **4**–**6** and related compounds are given in Table 3.

Looking at the data obtained, it is evident that the substitution of a silicon atom by a germanium results in a red-shift of the absorption band of the molecule. This could be explained by an effective conjugation between the identical atoms in the chain. A more significant shift is observed in the presence of aromatic substituents at Ge or Si centers.[9d,23,24] Increasing the number of atoms in the chain also resulted in a bathochromic shift. Furthermore, in the case of compound **6** the absorption band is clearly visible and may be due to an ideal conjugated structure similar to the one found in the crystal. At the same time, the nature of the substituting groups located at the end and in the center of the linear molecule clearly showed to impact on the UV/Vis absorption. On the one hand, electron-donating groups such as *p*-tolyl (when compared with phenyl) present at the ends of the chain resulted in a bathochromic shift. On the other hand, electron-withdrawing groups such as perfluorophenyl (when compared with methyl or phenyl) lead to an even more significant red-shift. Substitution on the central Ge atom (Me, Ph or *p*-Tol) has only a small effect on the absorption properties of the molecule. In conclusion, in solu-

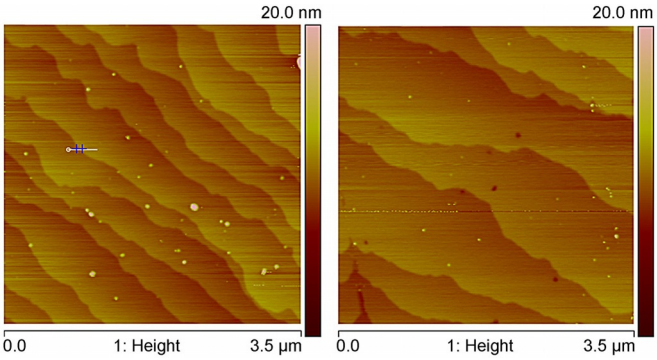

Figure 3. AFM image of different regions of compound **1**, single crystal surface.

Table 2. Structural parameters of compounds with a Ge-Si-Si-Ge chain.

Compound	d(Ge-Si)$_{av}$ [Å]	d(Si-Si) [Å]	Angle Ge-Si-Si [deg]	Torsion Ge-Si-Si-Ge [deg]	Reference
$[K(Me_3Si)_2Ge\text{-}SiMe_2\text{-}]_2$*2[18-crown-6]	2.429(2)	2.378(3)	116.05(10)	180	[18]
$[(Me_3Si)_3Ge\text{-}SiMe_2\text{-}]_2$	2.407(2)	2.379(2)	116.23(8)	180	[19]
$[(Me_3Ge)_3Ge\text{-}SiMe_2\text{-}]_2$	2.410(2)	2.349(3)	114.81(5)	180	[17]
$[(p\text{-}Tol)_3GeSiMe_2\text{-}]_2$ (**6**)	2.397(1)	2.349(2)	110.31(5)	180	this work

© 2017 Wiley-VCH Verlag GmbH & Co. KGaA, Weinheim

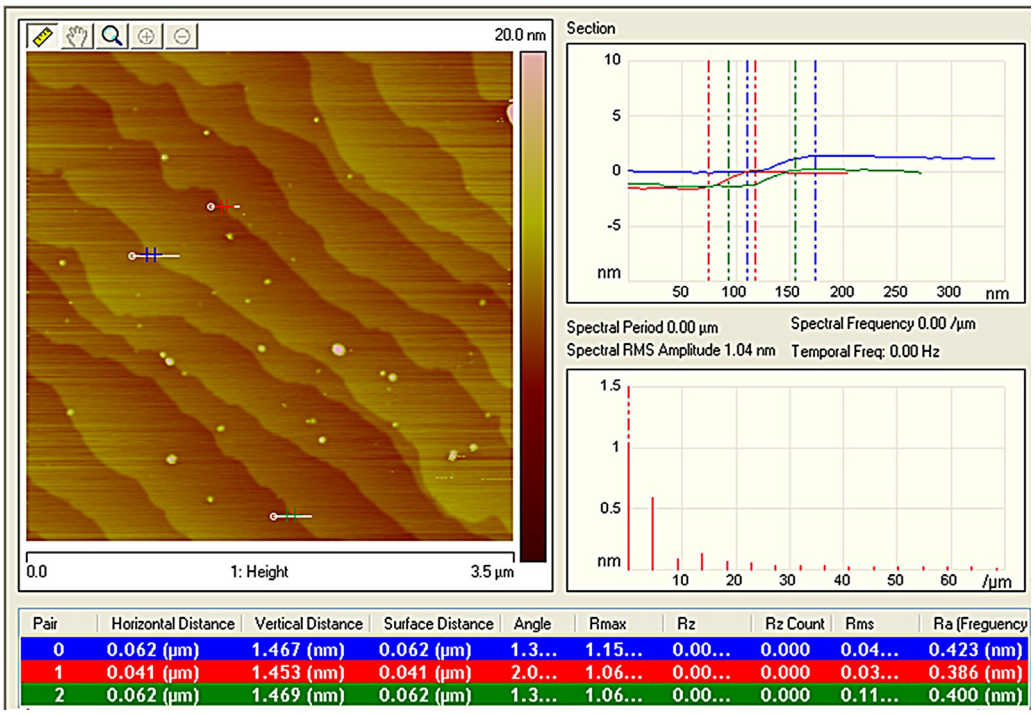

Figure 4. AFM image of the surface of compound **1,** single crystal and three surface profile cross-sections.

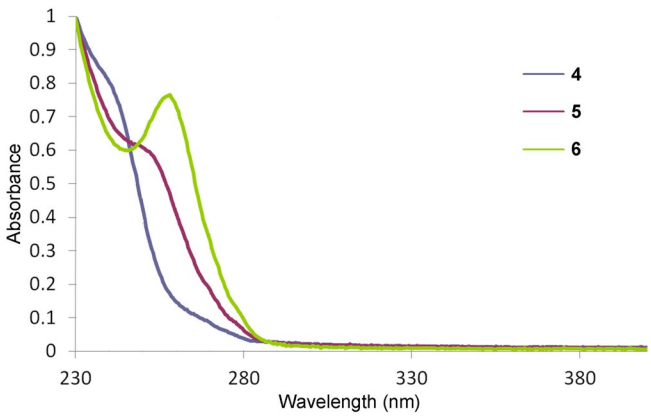

Figure 5. UV/Vis absorption spectra (normalized) for **4**–**6** in CH_2Cl_2.

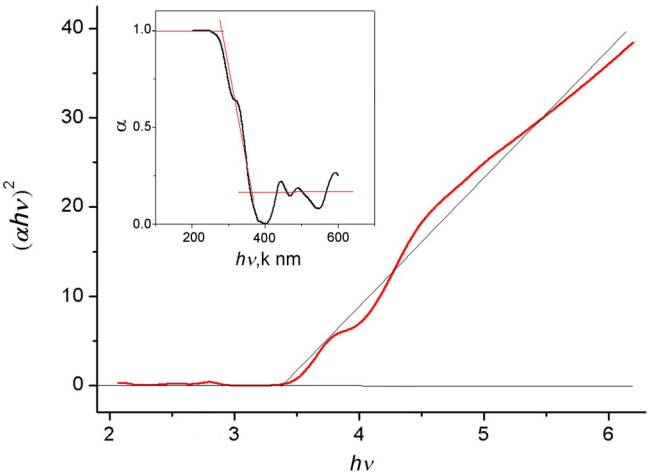

Figure 6. The plot of Kubelka–Munk function derivative for compound **3** used for the calculation of the optical band gap, E_g . Inset: spectral dependence of the absorption coefficient of compound **3** in the solid state.

tion, the substitution (group at E atom, nature of E) in the chains of group 14 elements significantly affects the UV/Vis absorption and may result in better conjugation between these atoms and in a bathochromic shift.

When moving from solution to the solid state, the compounds studied showed new optical properties. The absorption bands not only start at longer wavelengths but also display the characteristic shape of semiconductor absorption bands. The Kubelka–Munk plot for compound **3** is shown on Figure 6.

From this spectral dependence it is seen that a threshold wavelength exists below which the absorbance increases dramatically. Since the solid-state samples were powders or single crystals, the absorption spectra were recalculated from measured diffuse reflection.

The optical band-gap energy E_g of the solid samples was determined from the so-called intrinsic absorption edge. Several methods exist to accomplish this. The first method allowed us to make an approximate estimate of E_g directly from the plot of the absorption coefficient α. At high λ, the energy of a quantum is small and no absorption occurs. This corresponds to the right part of the curve shown in the inset of Figure 6. Once λ attains the critical value of λ_{edge}, the absorption abruptly rises. This means that a sharp kink of the $\alpha(\lambda)$ dependence occurs at $\lambda = \lambda_{edge}$ (see Figure 6, inset). The energy of a light quantum is related to the wavelength as $E = hc/\lambda = h\nu$.

© 2017 Wiley-VCH Verlag GmbH & Co. KGaA, Weinheim

Table 3. UV/Vis absorption for **4**–**6** and related compounds.

Compound	λ_{max}, nm [$\varepsilon \times 10^{-4}$, M^{-1} cm^{-1}]	Reference
Me_3Si-$SiMe_2$-$SiMe_3$	217 (0.8)	[20]
Me_3Ge-$GeMe_2$-$GeMe_3$	218 (0.8)	[21]
$PhMe_2Si$-$SiMe_2$-$SiMe_2Ph$	243 (1.95)	[22]
Ph_3Si-$SiPh_2$-$SiPh_3$	254 (3.22)	[22]
$(p\text{-Tol})_3Ge$-$SiMe_2$-$SiMe_3$ (**4**)	241 (2.5)	this work
$(p\text{-Tol})_3Ge$-$SiMe_2$-$SiMe_2$-$Ge(p\text{-Tol})_3$ (**6**)	258 (4.7)	this work
Ph_3Ge-$GeEt_2$-$GeEt_2$-$GePh_3$	256 (4.60)	[23]
Ph_3Ge-$GePh_2$-$GePh_2$-$GePh_3$	282 (4.5)	[11]
$(p\text{-Tol})_3Ge$-$GePh_2$-$GePh_2$-$Ge(p\text{-Tol})_3$	285	[16]
Ph_3Ge-$GeMe_2$-$GePh_3$	245 (3.02)	[23]
Ph_3Ge-$SiMe_2$-$GePh_3$	244 (4.42)	[23]
Ph_3Ge-$GePh_2$-$GePh_3$	250 (4.42)	[23]
Ph_3Ge-Ge(Me)Ph-$GePh_3$	250 (4.56)	[23]
$(p\text{-Tol})_3Ge$-$GeMe_2$-$Ge(p\text{-Tol})_3$ (**5**)	251 (4.0)	this work
$(p\text{-Tol})_3Ge$-$GePh_2$-$Ge(p\text{-Tol})_3$	251 (3.17)	[16]
$(p\text{-Tol})_3Ge$-$Ge(p\text{-Tol})_2$-$Ge(p\text{-Tol})_3$	253 (2.55)	[16]
$(p\text{-Tol})_3Ge$-$Ge(C_6F_5)_2$-$Ge(p\text{-Tol})_3$	258 (1.4)	[9d]

The main drawback of this approach lies in the difficulty to estimate correctly the absorption coefficient from scattering spectra. The α value of semiconductor materials varies within a wide range from 10^{-2} to 10^5 cm^{-1}. For this reason, when the absorption coefficient is measured, the thickness of a specimen is selected in such a manner that the absorbance $D=\alpha d$ (where d is the thickness of a specimen) is nearly equal to 1. In this case, it is possible to use, with an admissible error, the expression

$$T\ (1-R)^2 = \exp(-D),$$

which allows calculating the absorption coefficient from the measured R (Fresnel reflection coefficient), T (transmittance), and d as

$$\alpha = \frac{1}{d}\ln\frac{(1-R)^2}{T}$$

The situation becomes more complex for the detection of scattered radiation. Although no strict multiple scattering theory exists, the theory of the diffuse reflection and transmission of optically opaque specimens, i.e., the so-called two-component theory developed by Kubelka and Munk, is rather widely applied. For scattering specimens, this theory has the same importance as the Bouguer–Beer law in the absorption spectroscopy of transparent specimens. In the Kubelka–Munk theory, it is assumed that reflected radiation is isotropic, i.e., direction-independent, and radiating light is monochromatic. As a result of the solution of the Kubelka–Munk equation system, it turns out that the diffuse reflectance R_∞ of a specimen depends only on the ratio of the absorption coefficient α and the scattering coefficient S instead of either the scattering coefficient or the absorption coefficient, i.e.,

$$\alpha/S = (1-R_\infty)^2/2R_\infty = F(R_\infty)$$

The function $F(R_\infty)$ is called the Kubelka–Munk function. In diffuse reflection spectroscopy as well as in absorption and emission spectroscopy, the dependence of the response of an instrument on the wavelength must be eliminated. This is provided by measuring the diffuse reflection spectrum of a specimen itself, $\log R(\lambda)$, and the spectrum of scattering from an infinitely reflecting surface, $R_{ref}(\lambda)$, for instance, from a surface coated with a thin barium sulfate, magnesium carbonate, or magnesium oxide layer; here, the ratio is calculated in the logarithmic form $\log[R(\lambda)/R_{ref}(\lambda)]$. In the absence of reflection from the bottom part of a specimen (for example, when a specimen has a sufficient thickness for the light to be completely absorbed), it is equal to $\log R_\infty$. For the practical estimation of the band-gap energy in the case of direct interband transitions, the experimental data are expressed in the form of the dependence

$$(\alpha h\nu)^2 = A^2(h\nu - E_g),$$

which must be linear (Figure 6). As can be seen from Figure 6, the value of E_g is determined by extrapolating the linear dependence to the intersection with the abscissa axis.

The experimental dependence of α with $h\nu$ for indirect interband transitions is plotted in the form of curves $\sqrt{\alpha} = f(h\nu)$.

We analyzed the results using a variety of methods for determining the width of the forbidden zone. All our results proved that compounds **1**–**6** possess semiconductor properties. The values of band gap for those materials were in the range 3.3 ± 0.1 eV. According to DFT calculations for semiconductor polymers $[Ph_2Ge]_n$ the band gap width is 2.13 eV.[25] Furthermore, partial substitution of phenyl groups by protons, that is, $[Ph(H)Ge]_n$ and $[H_2Ge]_n$, results in 2.72 and 3.03 eV band gap width. This reveals the critical role of aryl groups (σ–π conjugation) in the band gap width value. The comparison with related silicon derivatives, $[Ph_m(H)_{2-m}Si]_n$, gives 3.61 ($m=2$), 3.72 ($m=1$) and 4.53 ($m=0$) eV,[26] or 3.5 eV for $[MePhSi]_n$[7] that reflects the role of the nature of the catenated atom in the chain.[9e] Therefore, we are confident that molecular oligogermanes, due to their physical properties, are promising semiconducting precursors.

In semiconducting organometallic compounds such as **1**–**6** the band gap is determined by the HOMO/LUMO gap. A decrease in the energy gap by varying the nature of the substituents (introduction of only electron-withdrawing substituents,[9d] or only electron-donating groups, substitution by Sn atoms[9e] or increasing the number of catenated atoms in the chain) should result in the appearance of bulk semiconductor properties.

The luminescent properties of compounds **2**–**6** were studied (Table 4) in solution (Figure 7) and in the solid state (Figures 8 and 9, Figure S18, Supporting Information).

The fluorescence of compounds **1**–**6** in solution shows that the electronic properties of the substituents on the Ge atom significantly affect the Stokes shift and the quantum yield. In-

© 2017 Wiley-VCH Verlag GmbH & Co. KGaA, Weinheim

Table 4. Fluorescence emission data for compounds **1**–**6**.

Compound	Solid State λ_{em} [nm][b]	Solution[a] λ_{em} [nm][b]	Φ_f [%][c]
Me_3Ge-Ge(*p*-Tol)$_3$ (**1**)[d]	357, 373, 393 (300)	286(270)	3.27
Ph_3Sn-Ge($SiMe_3$)$_3$ (**2**)	398 (350)	335 (285)	0.93
Ph_3Ge-Ge(C_6F_5)$_3$ (**3**)	373 (270)	377 (265)	12.50
(*p*-Tol)$_3$Ge-$SiMe_2$-$SiMe_3$ (**4**)	400 (290), 427 (370)	331, 350 (275)	10.64
(*p*-Tol)$_3$Ge-$GeMe_2$-Ge(*p*-Tol)$_3$ (**5**)	438 (380)	338 (285)	1.85
(*p*-Tol)$_3$Ge-$SiMe_2$-$SiMe_3$-Ge(*p*-Tol)$_3$ (**6**)	416 (300), 445 (320)	363, 375 (260)	1.98

[a] Spectra were recorded in CH_2Cl_2. [b] Excitation wavelength (λ_{ex}, nm) shown in parentheses. [c] Quantum yield. [d] The data from reference [9e].

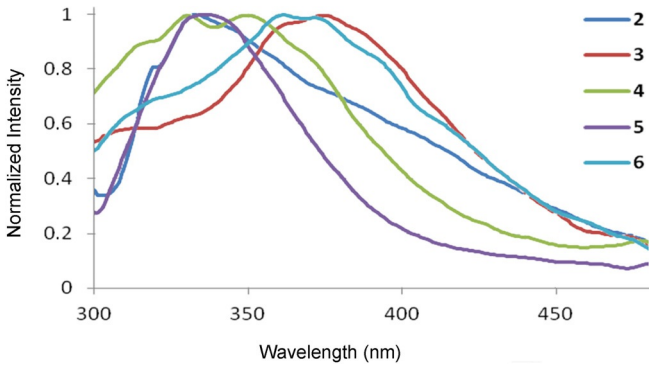

Figure 7. Emission spectra of compounds **2**–**6** in solution in CH_2Cl_2.

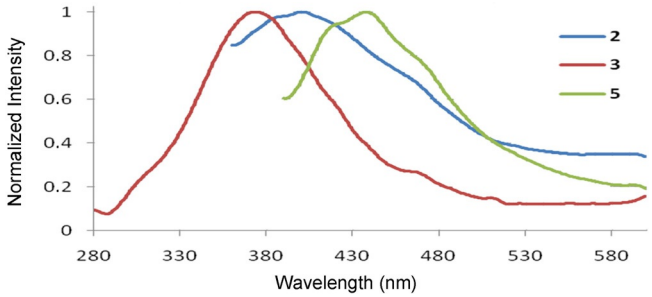

Figure 8. Emission spectra of compounds **2**, **3** and **5** in the solid state.

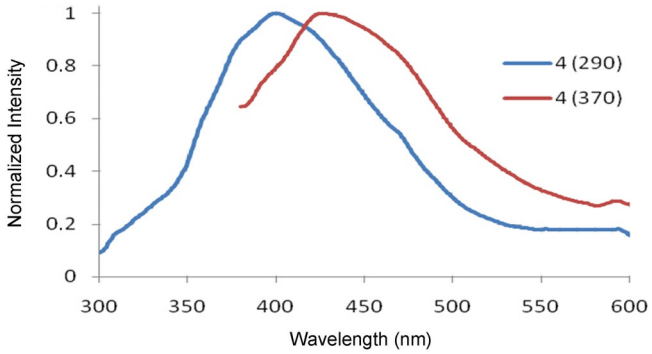

Figure 9. Emission spectra of compound **4** in the solid state at different excitation.

troduction of electron-withdrawing groups resulted in a red-shift with a high quantum yield. In the case of the silyl substituted derivatives, **4** and **6**, two emission bands were observed, indicating several excitation fragments.

On the contrary, in the solid state, silyl-substituted derivatives **4** and **6** showed only one fluorescence band. The emission wavelengths were red-shifted due to the strong interaction between molecules inside the molecular crystal in comparison with the results previously obtained in solution.

The studies presented in earlier research[8] has shown that the "conductance" of a molecule in solution could be measured by using a complex scanning tunneling microscope technique based on the break-junction (STM-BJ). Nevertheless, measures obtained by using this method are not representative of the physical properties of the bulk material. Most of the conductivity studies[6] carried out on polysilanes (polygermanes) used time-resolved methods (such as flash-photolysis time-resolved microwave conductivity (FP-TRMC) or time-of-flight (TOF) technique). Those studies have measured the intramolecular charge-carrier mobility and conductivity without predicting the carrier transport properties for long distances in the bulk material, and thus have only limited significance.

In this work, the conductivity study was carried out by using DC and AC conductivity techniques, as well as photoconductivity methods. Compounds **1**–**6** were analyzed as pellets made from the polycrystalline powder for **1**–**4** and single crystals for **1**, **5** and **6**. Furthermore, the doping procedure by iodination was used for compound **6**. All of the studied compounds have shown resistance typical of dielectric materials and no photoconductivity was observed. When compared to published data,[6d,8a,b] our results tend to indicate that the charge-carrier movements are hampered within the oligogermane molecules in the bulk material.

It is well known that the mobility of the charge carriers (usually holes in related compounds) strongly depends on the interfaces between molecules and between domains. In other words, the conductivity is determined by the structure of the material and decreases when increasing the number of domain borders.[27] There could be several reasons that might explain the low bulk conductivity and photoconductivity of the materials studied. The first possible reason is high energy barriers (either between molecules inside the material or at the contact point with the metallic electrodes) which may be preventing the charge carriers from moving. Also, a high number of the recombination centers can be present within the material itself. Nevertheless, it is safe to assume that the conductivity

© 2017 Wiley-VCH Verlag GmbH & Co. KGaA, Weinheim

could be improved by tweaking the oligogermanes. For instance, introducing a longer chain of σ-conjugated group 14 atoms or introducing novel substituents (like thiomethyl groups[8a,b]) on the Ge should improve the intermolecular electron transport and interaction with the electrodes and, therefore, this should result in observing an increase of the conductivity for these derivatives in the bulk material. Another way of solving this issue could be mixing the oligogermanes with an electron-transporting material such as fullerenes.[5]

To measure the level of HOMO (which correlates with the oxidation potential), electrochemical investigations were carried out for compound **2**, **3**, **4** and **6** under standard conditions in dichloromethane containing $[NBu_4][PF_6]$ (0.10 M) as supporting electrolyte. All data are referred to the standard for organometallic compounds, reference Fc/Fc^+. None of the compounds showed any cathodic reduction. Catenated aryl-substituted group 14 compounds are known to have irreversible oxidations[21,28] (equal to n−1 waves, where n is the quantity of *E* atoms in the chain),[16] since the *E*–*E* bonds are rapidly consequentially cleaved when oxidized.[9e,29] This differs from alkyl-substituted derivatives where only one oxidation wave is observed.

Compound **2** (Figure 10) showed a series of very close *chemically*-irreversible anodic oxidations at $E_{pa}=1.06$, 1.20, 1.41 and 1.62 V, respectively, vs. Fc/Fc^+ (approximately 1.55, 1.69, 1.90

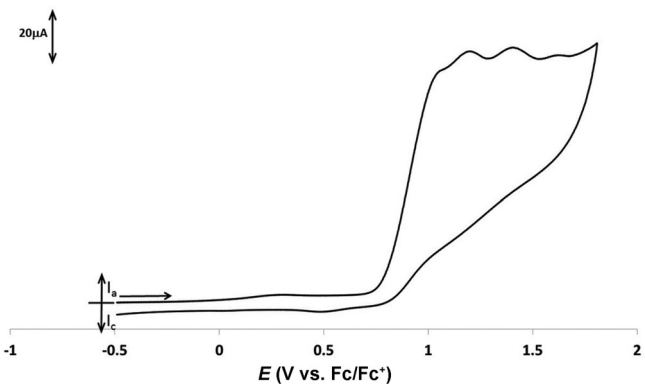

Figure 10. Cyclic voltammogram of 1 mM **2** in dichloromethane–$[NBu_4][PF_6]$ (0.1 M) solution. Sweeping rate of 200 mV s^{-1} at room temperature.

and 2.11 V vs. Ag/AgCl).[30] In addition, **2** displays an important degree of *electrochemical* irreversibility. The measured E_{pa}-$E_{pa/2}$ value for the first oxidation of **2** is diagnostic of a slow charge-transfer process with a coefficient (β) of 0.30.[31] No re-reduction wave was observed during the back scan due to the rapid chemical reaction occurring after the initial electron transfer (EC type).[32] Whilst the first anodic event could presumably be attributed to the oxidation of the Sn-Ge bond (compare with 1.52 V vs. Ag/AgCl for $(p\text{-Tol})_3GeSnMe_3$)[9] followed by the rapid cleavage of the formed radical cation,[9e] the subsequent oxidations encompass the oxidations of the decomposition products of the Sn–Ge radical cation as well as the Ge-Si bond oxidation. This anodic behavior differs significantly from what has been previously reported for other branched group 14 derivatives, where only one oxidation is observed.[30c,d]

The anodic electrochemistry of compounds **3** (Figure S19, Supporting Information) showed only one *chemically*-irreversible oxidation at $E_{pa}=1.62$ V vs. Fc/Fc^+ (approximately 2.11 V vs. Ag/AgCl). The presence of electron-withdrawing groups on the aromatic rings pushed the oxidation of the Ge–Ge bond to a very positive value and partially merges it with the solvent's wall; therefore, no charge transfer coefficient could accurately be measured. The introduction of an electron-withdrawing group within the core of **3** increases the oxidation potential by stabilizing the HOMO. Such a phenomenon is typically observed for oligogermanes containing a small number of element–element bonds.[9d]

Compound **4** (Figure 11) displayed two successive *chemically*-irreversible oxidations at $E_{pa}=1.01$, 1.30 V vs. Fc/Fc^+ (ap-

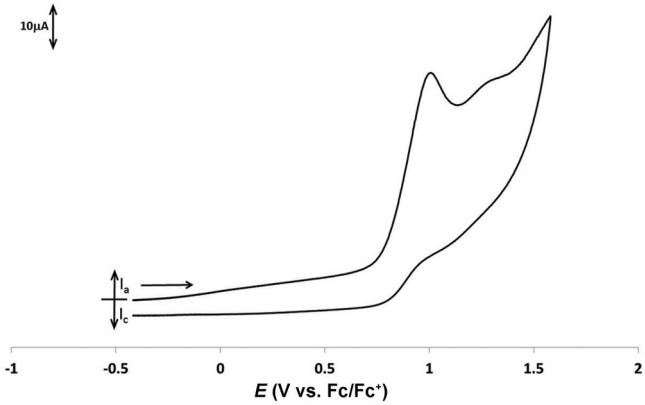

Figure 11. Cyclic voltammogram of 1 mM **4** in dichloromethane–$[NBu_4][PF_6]$ (0.1 M) solution. Sweeping rate of 200 mV s^{-1} at room temperature.

proximately 1.50, 1.79 V vs. Ag/AgCl). Again, the first oxidation displayed a slow electron transfer ($\beta=0.34$). It is safe to assume that the first anodic event is due to the oxidation of the Ge–Si bond. The second oxidation is either due to the presence of a decomposition product resulting from the rapid cleavage of the Ge–Si radical cation or to the oxidation of the Si–Si bond (compare with 1.79 V vs. Ag/AgCl for $(p\text{-Tol})_3GeSiMe_3$).[9] It is evident that elongation of the catenated atoms in the chain decreases the oxidation potentials (destabilizes the HOMO energy) and that the introduction of aryl groups on the E atoms stabilizes the radical cation.

Compound **6** (Figure S20, Supporting Information) displayed a series of successive ill-defined *chemically*-irreversible oxidations. Three oxidations appear at $E_{pa}=0.99$, 1.15 and 1.30 V vs. Fc/Fc^+ (approximately 1.48, 1.64 and 1.79 V vs. Ag/AgCl). Presumably, the first oxidation wave is due to the oxidation of the Ge–Si bond (compare with 1.01 V for **4**). The oxidation potential is shifted to a less positive value due to increased *E*–*E* chain length. Apparently, the second event is also due to Ge–Si bond oxidation in intermediate radical cation. The third process is typical for an Si–Si bond (compare with 1.30 V for **4**). The oxidation waves are too convoluted to allow measuring any charge-transfer coefficient accurately. No significant improvement of the resulting data was observed when the cyclic voltammetry experiments were conducted in dichloromethane

© 2017 Wiley-VCH Verlag GmbH & Co. KGaA, Weinheim

containing the weakly coordinating salt $[NBu_4][B(C_6F_5)_4]$ (0.05 M) as supporting electrolyte.[33]

The measured electrochemical data are in good agreement with what has been previously reported in the literature for similar compounds. Increasing the length of the catenated group 14 atoms chain decreases the first oxidation potential (1.79 V vs. Ag/AgCl for $(p\text{-Tol})_3GeSiMe_3$,[9e] 1.50 V for **4** and 1.48 V for **6**); in addition, branching of the structure resulted in a smaller increase of the oxidation potential (1.06 V for **2** and 0.99 V for **6**). Apparently, if the heavier E atom is present within the molecule, the first oxidation that occurs is the oxidation of the bond with this atom (Sn > Ge > Si; compare 1.52 V vs. Ag/AgCl for $(p\text{-Tol})_3Ge\text{-}SnMe_3$[9e] and 1.55 V for **2**).

Conclusions

We have disclosed improved structure–semiconductor property relationships for several oligogermanes as well as for several related silicon and tin compounds containing germanium. Although the overall conductivity of the bulk material remains an issue, we are confident that this problem could be solved by doping the material, by increasing the number of atoms in the catenated chain or by introducing functional groups (suitable for better interaction with the electrodes) on the germanium center.

Further studies on individual molecules similar to the ones reported in this work with known bulk (NMR, XRD, AFM) structure, optical (UV/Vis, luminescence) and electrochemical properties (CV) may open new possibilities and lead to new practical applications of catenated group 14 compounds.

Experimental Section

General methods and remarks. All operations with germanium derivatives were conducted in a dry argon atmosphere using standard Schlenk techniques. ^{1}H NMR (400.130 MHz), ^{13}C NMR (100.613 MHz), and ^{29}Si NMR (79.495 MHz) spectra were recorded on Bruker 400 or Agilent 400 spectrometers (at 295 K). Chemical shifts in the spectra are given in ppm relative to internal Me_4Si. Elemental analyses were carried out using a HeraeusVarioElementar instrument. UV/visible spectra were recorded using an Evolution 300 spectrophotometer (Thermo Scientific) with a cuvette of 0.10 cm path length. Fluorescence (room temperature) spectra were recorded with a Hitachi F-7000 spectrofluorimeter. Diffuse light scattering and adsorption was investigated with the use of an LS-55 PerkinElmer spectrophotometer. The surface structure of the obtained crystal was investigated using an "Multimode V" atomic force microscope (Production Veeco) in the tapping mode. DC conductivity and photoconductivity of the samples were measured with a Keithley 6487 picoammeter. AC conductivity and photoconductivity were measured by using an NR 4192 impedance analyzer. Silver epoxy paste was used to produce electric contacts to the samples. For the photoconductivity measurements, the samples were illuminated by using a 1 kW high-pressure xenon lamp (with white spectrum) through an MDR-12 monochromator. Mass spectra (EI-MS, 70 eV) were recorded on a Finnigan Mat Incos 50 quadrupole mass spectrometer with direct insertion; all assignments were made with reference to the most abundant isotopes.

Solvents were dried by usual procedures. Diethyl ether was stored under solid KOH and then distilled under sodium/benzophenone. *n*-Hexane was refluxed and distilled over sodium. Dichloromethane was distilled over CaH_2. C_6D_6 was distilled over sodium under argon. $CDCl_3$ was distilled over CaH_2 under argon.

*n*BuLi, $Me_3Si\text{-}Me_2SiCl$, $ClMe_2Si\text{-}Me_2SiCl$ were obtained commercially (Aldrich) and used as received. Compounds $(p\text{-Tol})_3GeH$,[34] Me_4Ge,[9e] $(p\text{-Tol})_3Ge\text{-}GeMe_3$ (**1**),[9e] $Ph_3Sn\text{-}Ge(SiMe_3)_3$ (**2**),[9e] $(C_6F_5)_3Ge\text{-}GePh_3$ (**3**)[9d] were synthesized according to literature procedures. Acetyl chloride was distilled over PCl_5 under a flow of argon.

Dimethyldichlorogermane, Me_2GeCl_2. An improved procedure was used.[35] Acetyl chloride (51.00 mL, 56.50 g, 720.00 mmol) was added dropwise to the mixture of Me_4Ge (26.00 g, 200.00 mmol) and anhydrous $AlCl_3$ (112.00 g, 840.00 mmol) at 0 °C under vigorous stirring. The reaction mixture was slowly warmed to room temperature and stirred for 5 h, then heated at 100 °C for 1 h. Volatile materials were distilled twice using an effective condenser, a giving colorless liquid, b.p. 120–123 °C, b.p.124 °C.[36] Yield: 18.40 g (53 %). ^{1}H NMR ($CDCl_3$, 400.130 MHz): $\delta = 1.20$ ppm (s, 6 H, CH_3). $^{13}C\{^1H\}$ NMR ($CDCl_3$, 100.613 MHz): $\delta = 10.77$ ppm (CH_3).

Dimethyl(tris(*p*-tolyl)germyl)trimethylsilylsilane, $(p\text{-Tol})_3Ge\text{-}SiMe_2\text{-}SiMe_3$ (4). *a) Synthesis of [tris(p-tolyl)germyl]lithium.* A solution of *n*BuLi in *n*-hexane (2.5 M, 0.46 mL, 1.15 mmol) was added dropwise to a solution of $(p\text{-Tol})_3GeH$ (0.40 g, 1.15 mmol) in diethyl ether (20 mL) at room temperature. The reaction mixture was stirred for 6 h. The solution of the lithium compound was used further without purification.

b) Synthesis of ***3***. A slution of $Me_3Si\text{-}Me_2SiCl$ (0.24 mL, 1.15 mmol) in diethyl ether (20 mL) was added dropwise to the ethereal solution of $(p\text{-Tol})_3GeLi$ obtained as described above. The reaction mixture was stirred overnight. Then water (20 mL) was added, the water phase was extracted with diethyl ether (3 × 20 mL), and the combined organic phases were dried over anhydrous Na_2SO_4. All volatile materials were removed under reduced pressure. The resulting residue was recrystallized from *n*-hexane. Compound **4** was isolated as a white microcrystal material, m.p. 80–81 °C. Yield: 0.32 g, 58 %. ^{1}H NMR ($CDCl_3$, 400.130 MHz): $\delta = 7.32$ (d, 6 H, $^3J_{H\text{-}H} = 7.8$ Hz, $p\text{-}C_6H_4$), 7.14 (d, 6 H, $^3J_{H\text{-}H} = 7.8$ Hz, $p\text{-}C_6H_4$), 2.35 (s, 9 H, $p\text{-}C_6H_4CH_3$), 0.33 (s, 6 H, $^2J_{H\text{-}29Si} = 3.1$ Hz, $SiMe_2$), −0.01 ppm (s, 9 H, $^2J_{H\text{-}29Si} = 3.1$ Hz, $SiMe_3$). $^{13}C\{^1H\}$ NMR ($CDCl_3$, 100.613 MHz): $\delta = 137.78$ (*ipso*-C_6H_4), 135.34, 128.87 (*p*- and *m*-C_6H_4) (aromatic carbons), 21.41 ($p\text{-}C_6H_4CH_3$), −1.46 ($SiMe_2$), −4.56 ppm ($SiMe_3$). One *ipso* aromatic carbon atom was not found due to overlapping with another signal. ^{29}Si NMR ($CDCl_3$, 79.495 MHz): $\delta = -15.36$ ($SiMe_3$), −38.94 ppm ($SiMe_2$). MS (EI, %): 477 ($[M^+]$, 17), 462 ($[M-Me]^+$, 4), 404 ($[M-SiMe_3]^+$, 11), 346 ($[Tol_3Ge]^+$, 100), 313 ($[M-SiMe_3-Tol]^+$, 16), 255 ($[Tol_2Ge]^+$, 41), 165 ($[TolGe+H]^+$, 17), 131 ($[Si_2Me_5]^+$, 12). UV (CH_2Cl_2), λ_{max}, nm (ε, $M^{-1}\,cm^{-1}$): 241 (2.5×10^4). Elemental analysis calcd for $C_{26}H_{36}GeSi_2$ (477.345): C 65.42, H 7.60. Found: C 65.24, H 7.49.

2,2-Dimethyl-1,1,1,3,3,3-hexakis(*p*-tolyl)trigermane, $(p\text{-Tol})_3Ge\text{-}GeMe_2\text{-}Ge(p\text{-Tol})_3$ (5). A solution of Me_2GeCl_2 (0.20 mL, 1.69 mmol) in diethyl ether (20 mL) was added dropwise to the ethereal solution of $(p\text{-Tol})_3GeLi$ obtained as described above from $(p\text{-Tol})_3GeH$ (1.17 g, 3.37 mmol) and *n*BuLi in *n*-hexane (2.5 M, 1.35 mL, 3.37 mmol). The reaction mixture was stirred overnight. Then water (20 mL) was added, the water phase was extracted with ether (3 × 20 mL), and the combined organic phases were dried over anhydrous Na_2SO_4. All volatile materials were removed under reduced pressure. The residue was recrystallized from a mixture of *n*-hexane/dichloromethane. Compound **5** was isolated as a white powder, m.p. 205–206 °C. Yield: 1.12 g, 84 %. ^{1}H NMR ($CDCl_3$, 400.130 MHz): $\delta = 7.18$ (d, 12 H, $^3J_{H\text{-}H} = 7.8$ Hz, $p\text{-}C_6H_4CH_3$), 7.03 (d,

© 2017 Wiley-VCH Verlag GmbH & Co. KGaA, Weinheim

12 H, $^3J_{H-H}$ = 7.8 Hz, p-$C_6H_4CH_3$), 2.35 (s, 18 H, p-$C_6H_4CH_3$), 0.59 ppm (s, 6 H, $GeMe_2$). $^{13}C\{^1H\}$ NMR ($CDCl_3$, 100.613 MHz): δ = 137.91, 134.65 (2 *ipso*-$C_6H_4CH_3$-p), 135.45, 128.87 (p- and m-$C_6H_4CH_3$) (aromatic carbons), 21.35 (p-$C_6H_4CH_3$), −2.14 ppm ($GeMe_2$). MS (EI, %): 795 ([M^+], 3), 780 ([M−Me]$^+$, 2), 449 ([M−$GeTol_3$]$^+$, 9), 346 ([Tol_3Ge]$^+$, 100), 255 ([Tol_2Ge]$^+$, 21), 165 ([TolGe+H]$^+$, 14). UV (CH_2Cl_2), λ_{max}, nm (ε, $M^{-1}cm^{-1}$): 251 (4.0×10^4). Elemental analysis calc. for $C_{44}H_{48}Ge_3$ (794.6819): C 66.50, H 6.09. Found: C 66.40, H 6.03.

1,1,2,2-Tetramethyl-1,2-bis[tris(p-tolyl)germyl]disilane, (p-Tol)$_3$Ge-SiMe$_2$-SiMe$_2$-Ge(p-Tol)$_3$ (6). A solution of $ClMe_2Si$-Me_2SiCl (0.12 mL, 0.64 mmol) in diethyl ether (20 mL) was added dropwise to the ethereal solution of (p-Tol)$_3$GeLi obtained as described above from (p-Tol)$_3$GeH (0.45 g, 1.30 mmol) and nBuLi in n-hexane (2.5 M, 0.52 mL, 1.30 mmol). The eaction mixture was stirred overnight. Then water (20 mL) was added, the water phase was extracted with ether (3×20 mL), and the combined organic phases were dried over anhydrous Na_2SO_4. All volatile materials were removed under reduced pressure. The residue was recrystallized from a mixture of n-hexane/dichloromethane. Compound **6** was isolated as a white powder, m.p. 233–234 °C. Yield: 0.32 g, 68%. ^1H NMR ($CDCl_3$, 400.130 MHz): δ = 7.32 (d, 12 H, $^3J_{H-H}$ = 7.8 Hz, p-$C_6H_4CH_3$), 7.15 (d, 12 H, $^3J_{H-H}$ = 7.8 Hz, p-C_6H_4), 2.37 (s, 18 H, p-$C_6H_4CH_3$), 0.23 ppm (s, 12 H, $SiMe_2$). $^{13}C\{^1H\}$ NMR ($CDCl_3$, 100.613 MHz): δ = 137.89, 135.22 (2 *ipso*-$C_6H_4CH_3$), 135.36, 128.93 (p- and m-$C_6H_4CH_3$) (aromatic carbons), 21.40 (p-$C_6H_4CH_3$), −3.03 ppm ($SiMe_2$). ^{29}Si NMR ($CDCl_3$, 79.495 MHz): δ = −34.66 ppm ($SiMe_2$). MS (EI, %): 809 ([M^+], 1), 687 ([M−2Me−Tol]$^+$, 1), 462 ([M−$GeTol_3$]$^+$, 41), 346 ([Tol_3Ge]$^+$, 100), 405 ([$Tol_3GeSiMe_2$]$^+$, 2), 255 ([Tol_2Ge]$^+$, 10). UV (CH_2Cl_2), λ_{max}, nm (ε, $M^{-1}cm^{-1}$): 258 (4.7×10^4). Elemental analysis calc. for $C_{46}H_{54}Ge_2Si_2$ (808.312): C 68.35, H 6.73. Found: C 68.23, H 6.68.

Electrochemistry. Electrochemical measurements were carried out using an Autolab 302N potentiostat interfaced through Nova 2.0 software to a personal computer. Electrochemical measurements were performed in a glovebox under oxygen levels of less than 5 ppm using solvent that had been purified by passing through an alumina-based purification system. Diamond-polished glassy carbon electrodes of 3 mm diameter were employed for cyclic voltammetry (CV) scans. CV data were evaluated using standard diagnostic criteria for diffusion control and for chemical and electrochemical reversibility. The experimental reference electrode was a silver wire coated with anodically deposited silver chloride and separated from the working solution by a fine glass frit. The electrochemical potentials are referenced to ferrocene/ferrocenium couple, as recommended elsewhere.[37] The ferrocene potential was obtained by its addition to the analyte solution.[38] At an appropriate time in the experiment, $[NBu_4][B(C_6F_5)_4]$ was prepared as previously described.[39]

X-ray crystallography. Experimental intensities were measured on a STADIVARI Pilatus (for **5** and **6**) diffractometer using the ω-scan mode. Absorption correction based on measurements of equivalent reflections was applied. The structures were solved by direct methods and refined by full matrix least-squares based on F^2 with anisotropic thermal parameters for all non-hydrogen atoms. All aromatic hydrogen atoms were placed in calculated positions. All H atoms were refined using a riding model. Details of X-ray studies are given in Table S1 (Supporting Information).

CCDC 1510022 and 1510023 contain the supplementary crystallographic data for this paper. These data can be obtained free of charge from The Cambridge Crystallographic Data Centre.

Acknowledgements

This work was financially supported by the Russian President Grant for Young Russian Scientists (MK-1790.2014.3—KVZ), in part by M.V. Lomonosov Moscow State University Program of Development (KVZ), Nazarbayev University (ORAU grant for Medicinal Electrochemistry—KL) and the Ministry of Education and Science of Kazakhstan (KL).

Keywords: luminescence · oligogermanes · organic semiconductors · silagermanes · X-ray analysis

[1] a) R. D. Miller, J. Michl, *Chem. Rev.* **1989**, *89*, 1359–1410; b) J. M. Zeigler, *Synth. Met.* **1989**, *28*, 581–591.
[2] a) C. Marschner, J. Hlina, in *Comprehensive Inorganic Chemistry II, 2nd ed.* (Eds.: J. Reedijk, K. Poeppelmeier), Elsevier, Amsterdam, **2013**, pp. 83–117; b) M. L. Amadoruge, C. S. Weinert, *Chem. Rev.* **2008**, *108*, 4253–4294; c) K. M. Baines, W. G. Stibbs, *Coord. Chem. Rev.* **1995**, *145*, 157–200.
[3] a) H. Teruyuki, U. Yuko, R. N. Prabhakar, T. Masato, *Chem. Lett.* **1992**, *21*, 647–650; b) R. West, *J. Organomet. Chem.* **1986**, *300*, 327–346.
[4] a) M. Abkowitz, M. Stolka, *Solid State Commun.* **1991**, *78*, 269–271; b) M. Abkowitz, M. Stolka, *J. Non-Cryst. Solids* **1989**, *114*, 342–344; c) Y. Kunimi, S. Seki, S. Tagawa, *Solid State Commun.* **2000**, *114*, 469–472; d) K. Mochida, S.-S. Nagano, *Inorg. Chem. Commun.* **1998**, *1*, 289–291.
[5] A. Feigl, A. Bockholt, J. Weis, B. Rieger in *Silicon Polymers* (Ed.: M. A. Muzafarov), Springer, Berlin, Heidelberg, **2011**, pp. 1–31.
[6] a) R. West, L. D. David, P. I. Djurovich, K. L. Stearley, K. S. V. Srinivasan, H. Yu, *J. Am. Chem. Soc.* **1981**, *103*, 7352–7354; b) K. Mochida, S. Maeyama, M. Wakasa, H. Hayashi, *Polyhedron* **1998**, *17*, 3963–3967; c) S. Shu, A. Anjali, K. Yoshiko, S. Akinori, T. Seiichi, M. Kunio, *Chem. Lett.* **2005**, *34*, 1690–1691; d) A. Acharya, S. Seki, A. Saeki, S. Tagawa, *Synth. Met.* **2006**, *156*, 293–297; e) S. Seki, A. Saeki, A. Acharya, Y. Koizumi, S. Tagawa, K. Mochida, *Radiat. Phys. Chem.* **2008**, *77*, 1323–1327.
[7] S. Nešpůrek, A. Eckhardt, *Polym. Adv. Technol.* **2001**, *12*, 427–440.
[8] a) R. S. Klausen, J. R. Widawsky, M. L. Steigerwald, L. Venkataraman, C. Nuckolls, *J. Am. Chem. Soc.* **2012**, *134*, 4541–4544; b) T. A. Su, H. Li, V. Zhang, M. Neupane, A. Batra, R. S. Klausen, B. Kumar, M. L. Steigerwald, L. Venkataraman, C. Nuckolls, *J. Am. Chem. Soc.* **2015**, *137*, 12400–12405; c) T. A. Su, H. Li, R. S. Klausen, J. R. Widawsky, A. Batra, M. L. Steigerwald, L. Venkataraman, C. Nuckolls, *J. Am. Chem. Soc.* **2016**, *138*, 7791–7795.
[9] a) K. V. Zaitsev, A. A. Kapranov, Y. F. Oprunenko, A. V. Churakov, J. A. K. Howard, B. N. Tarasevich, S. S. Karlov, G. S. Zaitseva, *J. Organomet. Chem.* **2012**, *700*, 207–213; b) K. V. Zaitsev, Y. F. Oprunenko, A. V. Churakov, G. S. Zaitseva, S. S. Karlov, *Main Group Met. Chem.* **2014**, *37*, 67–74; c) K. V. Zaitsev, A. V. Churakov, O. K. Poleshchuk, Y. F. Oprunenko, G. S. Zaitseva, S. S. Karlov, *Dalton Trans.* **2014**, *43*, 6605–6609; d) K. V. Zaitsev, A. A. Kapranov, A. V. Churakov, O. K. Poleshchuk, Y. F. Oprunenko, B. N. Tarasevich, G. S. Zaitseva, S. S. Karlov, *Organometallics* **2013**, *32*, 6500–6510; e) K. V. Zaitsev, E. K. Lermontova, A. V. Churakov, V. A. Tafeenko, B. N. Tarasevich, O. K. Poleshchuk, A. V. Kharcheva, T. V. Magdesieva, O. M. Nikitin, G. S. Zaitseva, S. S. Karlov, *Organometallics* **2015**, *34*, 2765–2774; f) K. V. Zaitsev, K. Lam, Z. Zhanabil, Y. Suleimen, A. V. Kharcheva, V. A. Tafeenko, Y. F. Oprunenko, O. K. Poleshchuk, E. K. Lermontova, A. V. Churakov, *Organometallics* **2017**, *36*, 298–309.
[10] a) C. S. Weinert, *Dalton Trans.* **2009**, 1691–1699; b) C. Marschner, J. Baumgartner, A. Wallner, *Dalton Trans.* **2006**, 5667–5674.
[11] S. Roller, D. Simon, M. Dräger, *J. Organomet. Chem.* **1986**, *301*, 27–40.
[12] M. Dräger, D. Simon, *J. Organomet. Chem.* **1986**, *306*, 183–192.
[13] K. Häberle, M. Dräger, *J. Organomet. Chem.* **1986**, *312*, 155–165.
[14] M. Weidenbruch, A. Hagedorn, K. Peters, H. G. von Schnering, *Chem. Ber.* **1996**, *129*, 401–404.
[15] M. Weidenbruch, A. Hagedorn, K. Peters, H. G. von Schnering, *Angew. Chem. Int. Ed. Engl.* **1995**, *34*, 1085–1086; *Angew. Chem.* **1995**, *107*, 1187–1188.

© 2017 Wiley-VCH Verlag GmbH & Co. KGaA, Weinheim

[16] M. L. Amadoruge, E. K. Short, C. Moore, A. L. Rheingold, C. S. Weinert, *J. Organomet. Chem.* **2010**, *695*, 1813 – 1823.
[17] J. Hlina, R. Zitz, H. Wagner, F. Stella, J. Baumgartner, C. Marschner, *Inorg. Chim. Acta* **2014**, *422*, 120 – 133.
[18] J. Fischer, J. Baumgartner, C. Marschner, *Organometallics* **2005**, *24*, 1263 – 1268.
[19] H. Wagner, J. Baumgartner, T. Müller, C. Marschner, *J. Am. Chem. Soc.* **2009**, *131*, 5022 – 5023.
[20] M. Shimizu, S. Ishizaki, H. Nakagawa, T. Hiyama, *Synlett* **1999**, 1772 – 1774.
[21] M. Okano, K. Mochida, *Chem. Lett.* **1990**, *19*, 701 – 704.
[22] H. Gilman, W. H. Atwell, P. K. Sen, C. L. Smith, *J. Organomet. Chem.* **1965**, *4*, 163 – 167.
[23] A. Castel, P. Riviere, B. Saintroch, J. Satge, J. P. Malrieu, *J. Organomet. Chem.* **1983**, *247*, 149 – 160.
[24] E. K. Schrick, T. J. Forget, K. D. Roewe, A. C. Schrick, C. E. Moore, J. A. Golen, A. L. Rheingold, N. F. Materer, C. S. Weinert, *Organometallics* **2013**, *32*, 2245 – 2256.
[25] W. Fa, X. C. Zeng, *Chem. Commun.* **2014**, *50*, 9126 – 9129.
[26] K. Takeda, H. Teramae, N. Matsumoto, *J. Am. Chem. Soc.* **1986**, *108*, 8186 – 8190.
[27] S. S. Lee, C. S. Kim, E. D. Gomez, B. Purushothaman, M. F. Toney, C. Wang, A. Hexemer, J. E. Anthony, Y.-L. Loo, *Adv. Mater.* **2009**, *21*, 3605 – 3609.
[28] K. Mochida, C. Hodota, R. Hata, S. Fukuzumi, *Organometallics* **1993**, *12*, 586 – 588.
[29] a) M. L. Amadoruge, J. R. Gardinier, C. S. Weinert, *Organometallics* **2008**, *27*, 3753 – 3760; b) C. R. Samanamu, M. L. Amadoruge, A. C. Schrick, C. Chen, J. A. Golen, A. L. Rheingold, N. F. Materer, C. S. Weinert, *Organometallics* **2012**, *31*, 4374 – 4385; c) C. R. Samanamu, M. L. Amadoruge, C. H. Yoder, J. A. Golen, C. E. Moore, A. L. Rheingold, N. F. Materer, C. S. Weinert, *Organometallics* **2011**, *30*, 1046 – 1058; d) C. R. Samanamu, N. F. Materer, C. S. Weinert, *J. Organomet. Chem.* **2012**, *698*, 62 – 65.
[30] In practical terms, electrochemical reversibility (also termed Nernstian behavior) refers to the speed of charge-transfer in a redox reaction, whereas chemical reversibility refers to follow-up reactions that accompany the charge-transfer process. For an introductory discussion of these terms, see A. J. Bard, L. N. Faulkner, *Electrochemical Methods, 2nd ed.*, Wiley, New York, **2001**, pp. 35 – 38 and pp. 44 – 49.
[31] a) A. J. Bard, L. N. Faulkner, *Electrochemical Methods, 2nd ed.*, Wiley, New York, **2001**, pp. 35 – 38 and pp. 236; b) D. A. Dickie, B. E. Chacon, A. Issabekov, K. Lam, R. A. Kemp, *Inorg. Chim. Acta* **2016**, *453*, 42 – 50.
[32] D. H. Evans, *Chem. Rev.* **1990**, *90*, 739 – 751.
[33] K. Lam, W. E. Geiger, *J. Org. Chem.* **2013**, *78*, 8020 – 8027.
[34] V. Y. Lee, H. Yasuda, M. Ichinohe, A. Sekiguchi, *J. Organomet. Chem.* **2007**, *692*, 10 – 19.
[35] H. Sakurai, K. Tominaga, T. Watanabe, M. Kumada, *Tetrahedron Lett.* **1966**, *7*, 5493 – 5497.
[36] H. Schumann, L. Esser, J. Loebel, A. Dietrich, D. van der Helm, X. Ji, *Organometallics* **1991**, *10*, 2585 – 2592.
[37] G. Gritzner, J. Kuta, *Pure Appl. Chem.* **1984**, *56*, 461 – 466.
[38] R. R. Gagne, C. A. Koval, G. C. Lisensky, *Inorg. Chem.* **1980**, *19*, 2854 – 2855.
[39] K. Lam, W. E. Geiger, *J. Organomet. Chem.* **2016**, *817*, 15 – 20.

Manuscript received: February 1, 2017
Accepted manuscript online: February 6, 2017
Version of record online: February 28, 2017

© 2017 Wiley-VCH Verlag GmbH & Co. KGaA, Weinheim